ADVANCED ENERGY MATERIALS
www.advenergymat.de

Highly-Safe and Ultra-Stable All-Flexible Gel Polymer Lithium Ion Batteries Aiming for Scalable Applications

Wei Shen, Ke Li, Yangyang Lv, Tao Xu, Di Wei, and Zhongfan Liu**

With the development of flexible electronics, flexible lithium ion batteries (LIBs) have received great attention. Previously, almost all reported flexible components had shortcomings related to poor mechanical flexibility, low energy density, and poor safety, which led to the failure of scalable applications. This study demonstrates a fully flexible lithium ion battery using $LiCoO_2$ as the cathode, $Li_4Ti_5O_{12}$ as the anode, and graphene film as the flexible current collector. The graphene oxide modified gel polymer electrolyte exhibits higher ionic conductivity than a conventional liquid electrolyte and improves the safety of the flexible battery. The optimum design of the flexible graphene battery exhibits super electrochemical performance, with a 2.3 V output voltage plateau and a satisfactory capacity of 143.0 mAh g^{-1} at 1 C. The mass energy density and power density are both ≈1.4 times higher than a standard electrode using metal foils as current collectors. No capacity loss is observed after 100 thousand cycles of mechanical bending. More importantly, even in the clipping state, this flexible gel polymer battery can still demonstrate a stable and safe electrochemical performance. This work may lead to a promising strategy of high-performance scalable LIBs for the next-generation flexible electronics.

1. Introduction

Flexible electronics are emerging and promising technologies for the next generation of deformable functional devices such as roll-up displays, smart electronics, and wearable electronic products.[1–5] The invention and applications of LIBs in the 20th century enabled people to enter a sustainable and cleaner society. With the 2019 Nobel Prize in Chemistry awarded to the three inventors of LIBs, it is believed that the use of LIBs in the field of deformable functional devices will become more and more popular. As the preferred power source for deformable functional devices, LIBs have many advantages over other rechargeable battery technologies, including relatively high energy and power densities, long cycling life, little memory effect, and low self-discharge.[6–8] When used in flexible electronics, LIBs need to be flexible, thin, stretchable, and even foldable.[9–11]

So far, flexible LIBs have been investigated for decades. Numerous strategies, such as fiber-shaped,[12] sponge-like,[13] spring-like stretchable,[14] and paper-like LIBs[15] have been reported, but none has been successful in real commercial applications. The reasons may be due to 1) low energy density, 2) poor mechanical flexibility, 3) poor safety, and 4) not being suitable for scalable applications. Presently, the development in the field of flexible LIBs is still at the early stage of research in laboratories, and most of the reports focus on flexible electrodes based on flexible current collectors.[13,15–18] Conventional metal foils (aluminum [Al] and copper [Cu]) as current collectors to support active materials[19] are unfit for flexible batteries because the active materials (cathode and anode) are easily delaminated from their smooth surface when the flexible batteries are bent. In addition, the high-density characteristics of metal restrict the mass energy density of LIBs. Therefore, replacing the metal foils with a highly conductive, light-weight, thin, and flexible current collector could enhance both the mass energy density and mechanical flexibility.

Recently, carbon-based materials featuring good electrical conductivity, high mechanical durability and low density are considered as the promising choice for current collectors in flexible LIBs.[20,21] The reported carbon based materials include carbon nanotubes (CNTs),[15,22–26] carbon cloth,[27] carbon fibers,[28] graphene based film,[29] and foam.[30,31] Thanks to the tremendous research efforts devoted over the past decades, research on flexible LIBs has made substantial progress. However, from the perspective of scalable applications, the above-mentioned carbon based materials still have some insurmountable problems. First, due to the difficult dispersion of CNTs and other nanocarbon materials in solution, the major challenge is to fabricate CNT films with uniform thickness and mass.[26] Although flexible CNT films can also be prepared directly through the floating-catalyst chemical vapor deposition (CVD) method at the high-temperature zone of the chamber with robustness and high conductivity, the area of the obtained films is limited by the diameter of the reaction chamber.[32,33] Second, for carbon cloth, there are numerous

Dr. W. Shen, K. Li, Y. Lv, T. Xu, Prof. D. Wei, Prof. Z. Liu
Beijing Graphene Institute
Beijing 100094, P. R. China
E-mail: weidi-cnc@pku.edu.cn; diwei@hotmail.com; zfliu@pku.edu.cn
Prof. Z. Liu
Center for Nanochemistry
Beijing Science and Engineering Center for Nanocarbons
Beijing National Laboratory for Molecular Sciences
College of Chemistry and Molecular Engineering
Peking University
Beijing 100871, P. R. China
The ORCID identification number(s) for the author(s) of this article can be found under https://doi.org/10.1002/aenm.201904281.

DOI: 10.1002/aenm.201904281

visual pores between the carbon fibers. As a result, the active materials can easily pass through when using the traditional electrode coating method. Consequently, hydrothermal method is required to adhere the active material on its surface. Such method has harsh synthesis conditions and cannot accurately control mass loading of active material, therefore, cannot be further scaled up.[27] Third, for carbon fibers, it is usually made into fiber-shaped LIBs.[12] Because the weight of active materials supported by carbon fibers is limited, the energy density of fiber-shaped LIBs is lower than that of other shaped flexible LIBs. Finally, for graphene foam, the costly CVD method is also required to grow 3D conductive interconnected graphene network. Moreover, in order to embed active materials inside the CVD graphene foam, hydrothermal method is again required to in situ grow the active materials.[31] These are not suitable for scalable applications in the field of LIBs at present. Although the above-mentioned carbon-based materials showed excellent flexibility as current collectors, they are still not satisfactory enough to meet practical needs and are difficult to achieve scalable applications. Therefore, developing a solution to realize scalable production and fabrication of flexible batteries is urgently desirable.

Safety is always a critical concern for LIBs, and it becomes even more challenging for flexible LIBs. Presently, most reported flexible LIBs employ organic carbonate solvent and polyolefin-based separators. In the bending process of the flexible battery, the liquid electrolyte has strict requirements on the packaging material due to its fluidity. Once the packaging material is broken, the leakage of electrolyte and short circuit of the battery will result in a huge safety hazard. Some catastrophic accidents have happened owing to using liquid electrolyte and the polyolefin-based separators, such as spontaneous combustion of Samsung Note 7 and Tesla Model S in 2019.[34,35] On the other hand, gel polymer electrolyte (GPE) is attracting strong interests and regarded as a promising candidate to solve the potential safety issues of LIBs.[36] Compared with liquid electrolytes, GPEs have several advantages as a membrane in terms of no internal shorting, no leakage of liquid electrolytes, and nonflammability.[37,38] As GPEs, poly(ethylene oxide) (PEO),[39] poly(acrylonitrile) (PAN),[40] poly(vinyl chloride) (PVC),[41] poly (methyl methacrylate) (PMMA),[42] and polyvinylidene difluoride (PVDF)[43] have been studied extensively. However, some shortcomings such as relatively low ionic conductivity, poor mechanical strength and narrow electrochemical window limit their further applications.[44,45] In order to address above-mentioned issues, there has been an ongoing research to improve the overall performance of GPEs. Despite the great efforts in the past few decades, the overall performance is still not satisfactory. Therefore, it is very important to exploit a new type of GPE with satisfactory comprehensive performance.

In this study, we demonstrate a flexible rechargeable LIB designed for future scalable applications using flexible graphene film as a current collector and a new GPE made of graphene oxide (GO)-modified poly(vinylidene fluoride-tri-fluoroethylene-chlorofluoroethylene) (PTC). The graphene electrode exhibits excellent flexibility and is resistant to delamination of active materials even when the battery is folded repeatedly. Furthermore, to the best of our knowledge, LIBs using PTC-based GPE as a new type of material have so far been barely reported. Compared with the dielectric constant of previously reported PE (2.3), PP (2.2–2.3), PEO (≈5), PAN (5.5), PMMA (3.0), and PVDF (8.15–10.46), the higher dielectric constant of PTC (50–57) is critical to GPE through improving dissociation degree of $LiPF_6$.[46] Increasing dissociation degree of $LiPF_6$ can further increase ionic conductivity of GPE. Only if the ionic conductivity of GPE is comparable to that of liquid electrolyte, it is possible to make it have a commercial application prospect. In this study, it is demonstrated that after further modification of GO, PTC-based GPE exhibits superior ionic conductivity than liquid electrolytes. Moreover, strong absorption of liquid electrolyte, superior mechanical strength, and high electrochemical stability have also been achieved. Finally, according to the above components, we show a full cell using GO-modified PTC based GPE and graphene film as a current collector for both LCO cathode and LTO anode. The flexible LIBs not only exhibit high electrochemical stability even after 100 thousand times mechanical bending, but also still work even under the condition of a corner being cut away.

2. Results and Discussion

2.1. Flexible Current Collectors

The method of coating slurry of active materials on current collectors is the simplest and most effective way for electrode preparation and has been widely used in the preparation of commercial LIBs. The adhesion between the active material layer and the current collector is important to structural stability of electrode when the battery is mechanically bent.[24] The adhesion is influenced by the morphology of active materials and surface characteristics of current collectors. The scanning electron microscopy (SEM) of the active materials (LCO and LTO) is shown in Figure S1, Supporting Information. Figure S1a,b, Supporting Information, shows the morphology of LCO is single crystal and the average particle size is in the range of 5–15 μm. The wide particle size distribution could improve the compaction density of the electrode and therefore could contribute strong adhesion to graphene film. Similar to LCO, LTO consisted of spherical secondary particles, which had a wide particle size distribution in the range of 10–40 μm.

In addition to the wide particle size distribution of LCO and LTO, the rough surface of graphene film also contributed to increased contact area between the electrode and the current collector, and therefore significantly increased adhesion, as shown in **Figure 1**a.[47] Figure 1b shows the cross-sectional SEM images of the graphene film. Graphene sheets tend to orderly stack to form an electrically conductive structure, which is generally higher than the electrical conductivity of the reported CNT film,[48] with unilateral electrical conductivity and rGO[49] material. This ordered stacking helps to make the thickness and weight of graphene film more uniform, as shown in Tables S1 and S2, Supporting Information. The uniformity of thickness and weight for current collector is the foundation of scalable applications. Thickness tests by digimatic indicator were performed at random locations on the graphene film, Al foil, and Cu foil (Table S1, Supporting Information). As can be seen, the thickness of graphene film is relatively uniform compared to

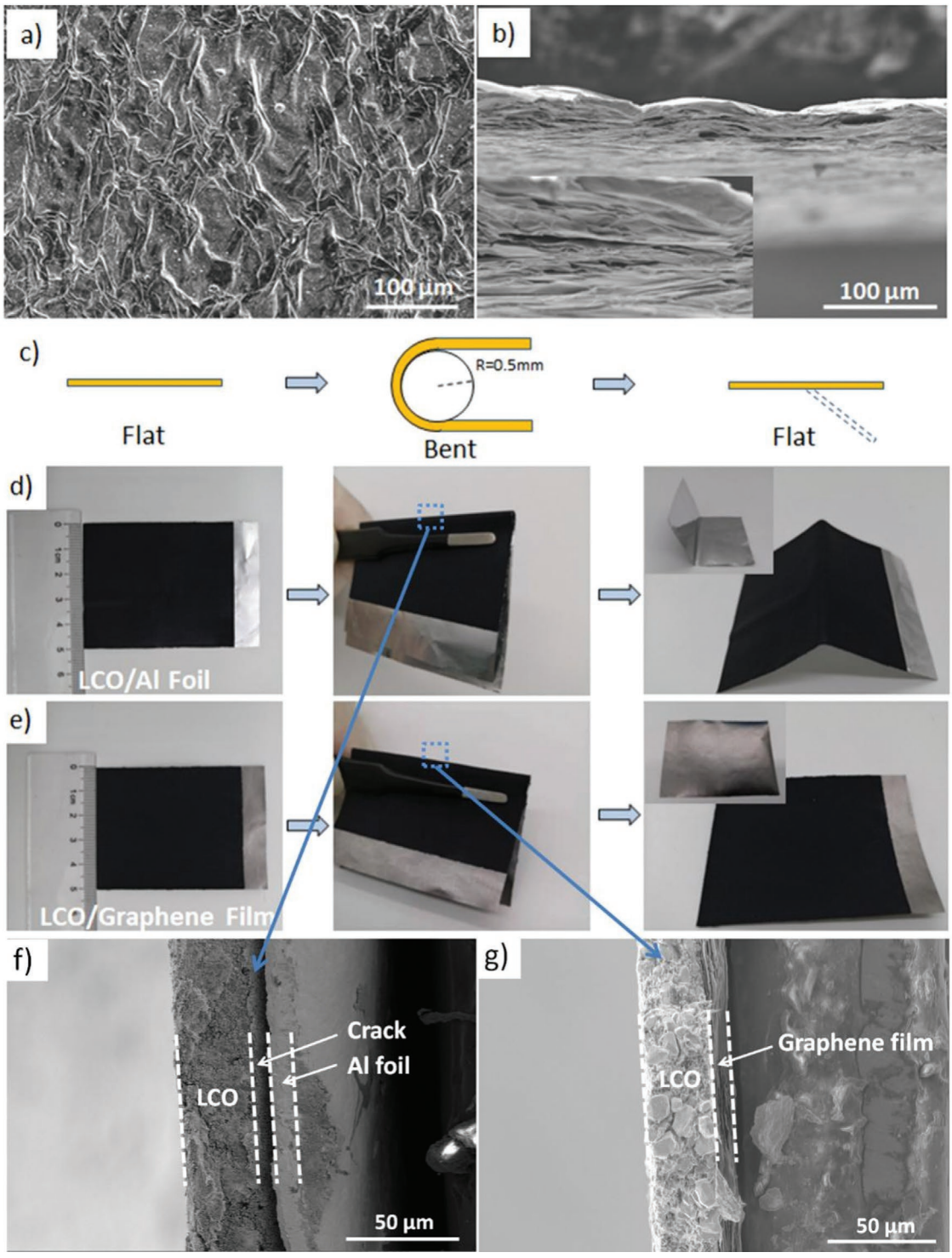

Figure 1. a) SEM image of surface morphology and b) cross-sectional SEM image of graphene film. c) Schematic diagram of flexible electrode bending. Picture of electrode bending for d) LCO/Al Foil and e) LCO/graphene Film. Cross-sectional SEM images of crease for f) LCO/Al Foil and g) LCO/graphene Film electrodes.

Al foil and Cu foil, and the average thickness is about ≈11 µm. Compared with Al foil and Cu foil, graphene film shows a lower thickness (≈11 µm) than Al foil (≈16 µm) and a similar thickness to Cu foil (≈10 µm). When replacing the metal foils with graphene film as the current collector both for the cathode and the anode, the LIBs will exhibit a higher volume energy density. Furthermore, the densities of graphene film, Al foil, and Cu foil were also calculated and the values were 2.19, 2.66,

and 8.85 g cm^{-3}, respectively. The lower density of graphene film contributes to the enhancement in mass energy density of LIBs. The mass energy density and power density of the as-fabricated flexible electrodes using graphene film in this study were 108 Wh kg^{-1} and 143 W kg^{-1}, respectively, far more than the values of 79 Wh kg^{-1} and 105 W kg^{-1} when using charge collectors of metal foils. Moreover, the mass energy densities for flexible LIB full cells were 68.8 and 59.9 Wh kg^{-1} when using graphene film and metal foils as the current collectors, respectively.

The photographs of flexibility comparison for LCO cathode coated on both Al foil (LCO/Al Foil) and graphene film (LCO/Graphene Film) with the bending radius of 0.5 mm are presented in Figure 1d,e. As can be seen, LCO/Graphene Film electrode shows more deformable capability than LCO/Al Foil electrode. Moreover, in order to further explore the morphological characteristics of the flexible electrodes, SEM images on the region of electrodes under stress were taken, as displayed in Figure 1f,g. As can be seen, no delamination occurred on LCO/Graphene Film but it is clearly shown on LCO/Al Foil, demonstrating its superior mechanical flexibility when using graphene film as current collector. Such enhancement in flexibility and strong adhesion will stabilize electrochemical performance during bending tests.

The electrochemical performances of all electrodes were investigated using a half-cell configuration with lithium metal as the counter electrode in a coin cell in Figure S2, Supporting Information. The charge/discharge curves of LCO and LTO electrodes at 0.2 C are shown in Figure S2a,d, Supporting Information. In this work, 1 C = 163.3 mA g^{-1} for LCO electrode and 1 C = 170 mA g^{-1} for LTO electrode. The LCO electrode was cycled in the voltage window of 3.0–4.4 V (vs Li/Li^+) and the LTO electrode was cycled in the voltage window of 1.0–2.5 V (vs Li/Li^+). Apparently, the charge/discharge curves, rate performance, cycle performances, and coulombic efficiency of LCO and LTO electrodes using graphene current collectors well matched the results using metal current collectors, indicating comparable conductivity of the graphene film with metals. Therefore, based on the sufficient conductivity, strong adhesion, and strong mechanical flexibility, it is easy to understand why graphene film will exhibit superior electrochemical performance in flexible LIBs. The graphene films could be mass produced with low cost, which is critical for the scalable applications of flexible batteries in the future.

2.2. PTC-Based Gel Polymer Electrolyte

Thermal shrinkage of the separator is a vital aspect to evaluate safety characteristics of the LIBs. The dimensional changes of Celgard separator, pristine PTC/PEO gel polymer electrolyte (P-GPE), and GO-modified PTC/PEO gel polymer electrolyte (GO-GPE) before and after thermal treatment at 140 °C for 1 h are shown in **Figure 2** insets, and the surface structure and morphology are shown in Figure 2. It can be easily found that Celgard separator suffered a drastic dimensional reduction, and the pore diameter significantly reduced after the thermal treatment. Compared with the Celgard separator, the 3D porous structure and the pore diameter of P-GPE and GO-GPE almost had no significant change after thermal treatment (Figure 2c–f). In addition, the dimension of P-GPE and GO-GPE still remained unchanged after thermal treatment (insets of Figure 2c–f). Moreover, the higher temperature of 160, 180, and 200 °C treatments for 1 h were also carried out for GO-GPE. When the treatment temperature is not higher than 160 °C, the pore diameter and dimension of PTC membrane are stable; otherwise, the pore diameter will contract sharply as shown in Figure S3b,c, Supporting Information. The excellent thermal stability of the porous PTC membrane was due to that PTC has a higher softening temperature than polyethylene (PE), which is the main constituent substrate of the Celgard separator. In addition, GO could also effectively enhance the mechanical property and thermal stability of the polymer.[50]

In order to further investigate the thermal stability of various membranes, burning experiments were carried out and shown in Figure S4, Supporting Information. GO-GPE exhibits excellent flame retardancy; in contrast, the commercial Celgard separator is easily burnt. This is because GO-GPE contains halogen atoms (F and Cl) which have effective flame retardancy. Moreover, the addition of GO also can enhance flame retardancy of polymer-based composites to some extent and has been proved in some recent work.[47,51,52] Furthermore, it should be noted that after the addition of GO, the distribution of the pores becomes more uniform with higher density, and the pore size becomes smaller as shown in Figure 2c. The smaller pore size contributes to prevent the direct passage of the electrode particles and thus to avoid the micro-short circuit between anode and cathode. The improvement of pore configuration may be due to the following factors: First, as shown in Figure S5, Supporting Information, GO contains a large number of oxygen-containing functional groups, such as C—O (286.4 eV), C=O (287.7 eV), and O—C=O (288.8 eV). Among them, the peak area of C—O is the largest, indicating C—O is the majority of oxygen-containing groups in GO. The —OH (C—O) and —COOH (O—C=O) can easily produce intermolecular hydrogen bonding with polymer matrices, resulting in more disordered polymer chains in the composites, which helps to form a 3D porous polymer network.[53] Second, polymer molecular chains could be immobilized easily by hydrogen bonding and the 3D skeleton of GO to form uniform pore structures during phase inversion,[54] which is due to the homogeneous dispersion of GO in the slurry of GO-GPE.

The smaller pores of GO-GPE compared to P-GPE could remarkably enhance specific surface area, as shown in Figure S6a, Supporting Information. The specific surface area for P-GPE is 4.04 m^2 g^{-1} and it increases to 5.28 m^2 g^{-1} for GO-GPE. This contributes to increase in the liquid electrolyte uptake when using GO-GPE (Figure S6b, Supporting Information). Compared with the electrolyte uptake (186%) of the P-GPE, the electrolyte uptake of GO-GPE increases to 277%. This means that GO-GPE could wet more easily in liquid electrolytes and retain the electrolytes more permanently than those of P-GPE, which can facilitate the improvement in ionic conductivity and cycle stability of batteries.

Ionic conductivity is considered as a key factor of GPEs. According to Equation (1), the ionic conductivities of Celgard separator, P-GPE, and GO-GPE are calculated and the values of 1.25×10^{-3}, 2.03×10^{-3}, and 2.28×10^{-3} S cm^{-1} are shown in

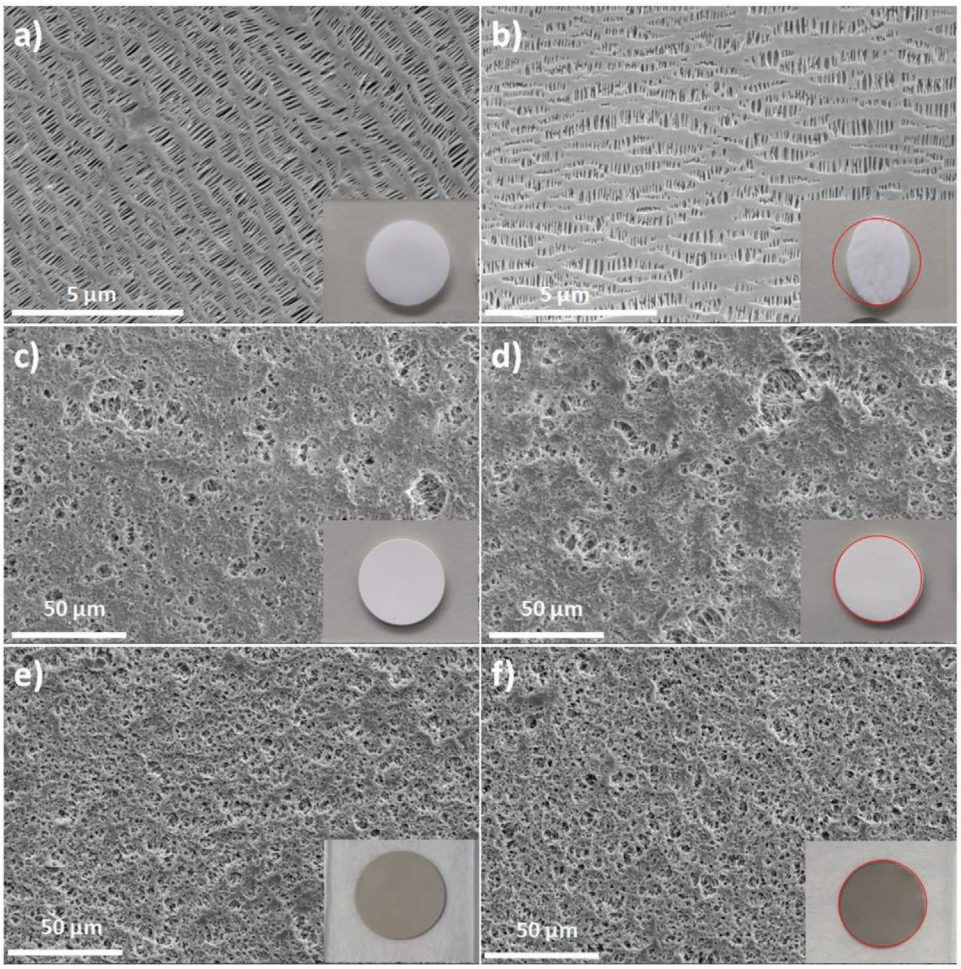

Figure 2. SEM images of commercial Celgard separator (a,b), P-GPE (c,d), and GO-GPE (e,f), before (a,c,e) and after (b,d,f) thermal treatment at 140 °C for 1 h (inset: corresponding photographs).

Figure 3a. It is observed that PTC-based GPE exhibits higher ionic conductivity than Celgard separator. The reasons may be due to : 1) PTC has a high dielectric constant (50–57)[46] than polyethylene of Celgard separator (2.26–2.4).[55] This can generate a large quantity of charge carriers by effectively dissociating $LiPF_6$,[56] thus improving the ionic conductivity of PTC-based GPE. 2) The Li^+ can only be transported in the amorphous region of GPE but not in the crystallization zone. The addition of PEO could reduce the crystallinity of PTC due to the hydrogen bond interaction effect between PTC and PEO.[45] Therefore, the ionic conductivity of PTC-based GPE increases. Furthermore, the ionic conductivity of GO-GPE achieved the highest value among all the samples. The further improvement in ionic conductivity by GO additives may be due

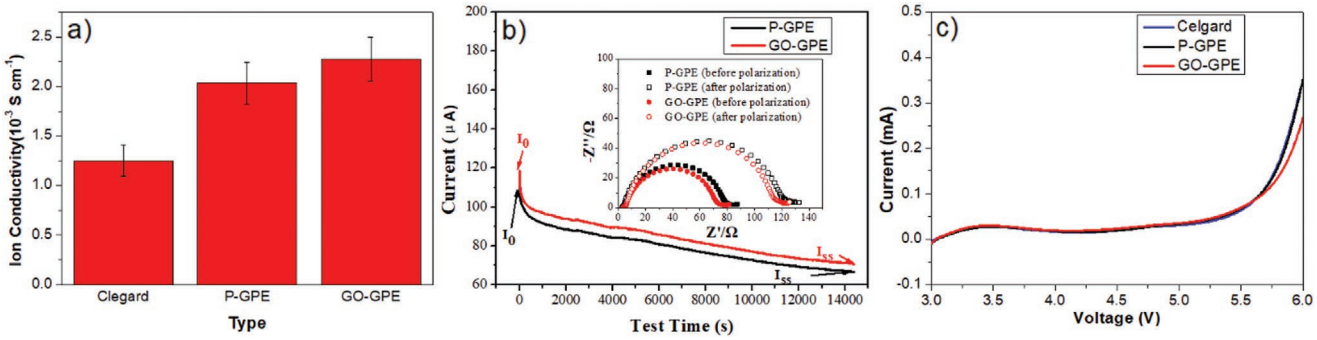

Figure 3. a) Ion conductivity of Celgard separator and various GPEs. b) Chronoamperometry profiles of Li|P-GPE|Li and Li|GO-GPE|Li cells at 25 °C; the inset is electrochemical impendence spectrum at 25 °C. c) The linear sweep voltammograms (LSV) curves of Celgard separator and various GPEs.

to the following aspects: 1) The increase in the liquid electrolyte uptake in the pores of GO-GPE could enable liquid electrolyte to penetrate into the polymer chains to swell the amorphous domains.[57,58] 2) The electrostatic interaction between the oxygen-containing functional groups with unshared electron pairs on GO and Li^+ are supposed to facilitate desolvation of Li^+.[59] 3) The electron deficiency of the carbon grid in GO could attract and immobilize PF_6^- anions. Moreover, —OH and —COOH groups of GO can also immobilize the PF_6^- anions by the hydrogen bonding, resulting in the destruction of the ion-solvent clusters and the formation of space charge layers, thus promoting the transport of Li^+.[59,60] 4) The possible interactions between GO and the fluorine functionalities in PTC that will further increase the degree of the electron deficiency in the carbon grid.[60]

In addition, the lithium ion transference number (t_{Li}^+) relative to ionic conductivity is critical for electrochemical performance of GPEs. The t_{Li}^+ was tested by assembling the coin cell with a symmetrical structure of Li|GPE|Li and further characterized by chronoamperometry and EIS tests (Figure 3b).[61] The t_{Li}^+ value of P-GPE is 0.459, which can be calculated by the Equation (2). Meanwhile, the GO-GPE achieved a more satisfactory t_{Li}^+ value of 0.599, which is obviously larger than P-GPE without GO. The improvement in ionic conductivity and t_{Li}^+ can ensure better electrochemical performance of the battery. Furthermore, Figure 3c shows the electrochemical stability window of Celgard separator, P-GPE, and GO-GPE evaluated by a linear sweep voltammetry (LSV) method, which used stainless steel (SS)|GPE|Li and SS|Celgard|Li cell. No anodic currents were observed below 5 V versus Li^+/Li for Celgard separator, P-GPE, and GO-GPE. The results indicate that PTC-based GPE possesses wide electrochemical stability window and can be applicable to LIBs.

In order to further prove the electrochemical stability of PTC-based GPE, CV was also performed in the voltage window of 3.0–4.3 V at the scanning rate of 0.1 mV s^{-1} by using LCO and lithium foil as the cathode and the anode, respectively (Figure S7, Supporting Information). It can be seen that there is no excess redox peak in GPEs compared to Celgard separator, which further proved the stability of PTC-based GPE in LIBs.

The electrochemical performances of as-fabricated LCO-Al Foil half cells using Celgard separator, P-GPE, and GO-GPE in the voltage window of 3.0–4.3 V (vs Li/Li^+) are shown in **Figure 4**. Before electrochemical experiments, Celgard separator and GPEs were both heated at 25 and 140 °C for 1 h, and then the half cells were assembled and tested at 25 °C. Under 25 °C, the half cells of various membranes all exhibit excellent rate performance at 0.4, 2, and 4 C (inset in Figure 4a) and stable cycle performance at lower current density of 1 C (Figure 4b). The capacity retention of Celgard separator, P-GPE, and GO-GPE are 95.2%, 95.6%, and 97.6%, respectively. However, when the current density increases to 4 C, the cycle performances of PTC-based GPEs are obviously better than Celgard separator, as shown in Figure 4a. Moreover, GO-GPE exhibits the best cycle stability. The initial discharge capacity of 117.9 mAh g^{-1} is obtained. After 170 cycles, the discharge capacity is still as high as 104.4 mAh g^{-1}, and the capacity retention is approximately 88.5%. However, the capacity retentions of Celgard separator and P-GPE are only 49.5% and 76.9%, respectively. When the heat treatment temperature increases to 140 °C, the Celgard separator suffers a drastic dimensional reduction, resulting in short circuit and the half cell cannot work. In contrast, the rate performances of PTC-based GPEs after the heat treatment of 140 °C barely changes. Moreover, the GO-GPE exhibits excellent cycle stability at 4 C with capacity retention of 74.3% at the heat treatment at 140 °C. The above results indicate that GO-GPE plays an important role in improving the safety and cycle stability of LIBs, which are attributed to the high thermostability, improved electrolyte uptake, excellent ionic conductivity, and lithium ion transference number mentioned earlier.

2.3. Flexible Lithium Ion Batteries

After studying the half cell performance, the electrochemical study of pouch-type flexible full cells were also investigated. The flexible full cell, denoted as LIB-Graphene Film, was assembled using graphene film as current collector and optimal GO-GPE. For comparison, a controlled full cell, denoted as LIB-Metal Foil, was also assembled using standard current collectors (Al foil and Cu foil) and GO-GPE. Nickel and aluminum tabs were used to make electric contact to the current collector.

In order to further analyze the effect of mechanical flexibility on the structural changes within the reinforced electrodes, electrochemical impedance spectroscopy (EIS) measurements were performed, as shown in **Figure 5**. Figure 5a,b shows the Nyquist plots, which were collected in a 5 mV AC potential signal in the

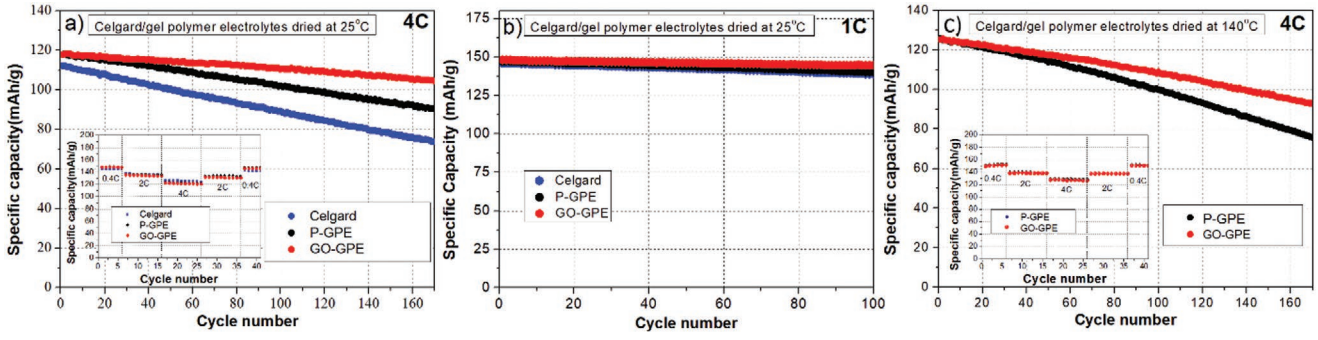

Figure 4. Celgard and various GPEs were dried at a,b) 25 °C or c) 140 °C for 1 h. Then cycle and rate (inset) performances of LCO-Al Foil hall cell using the treated Celgard and GPEs were tested at 25 °C.

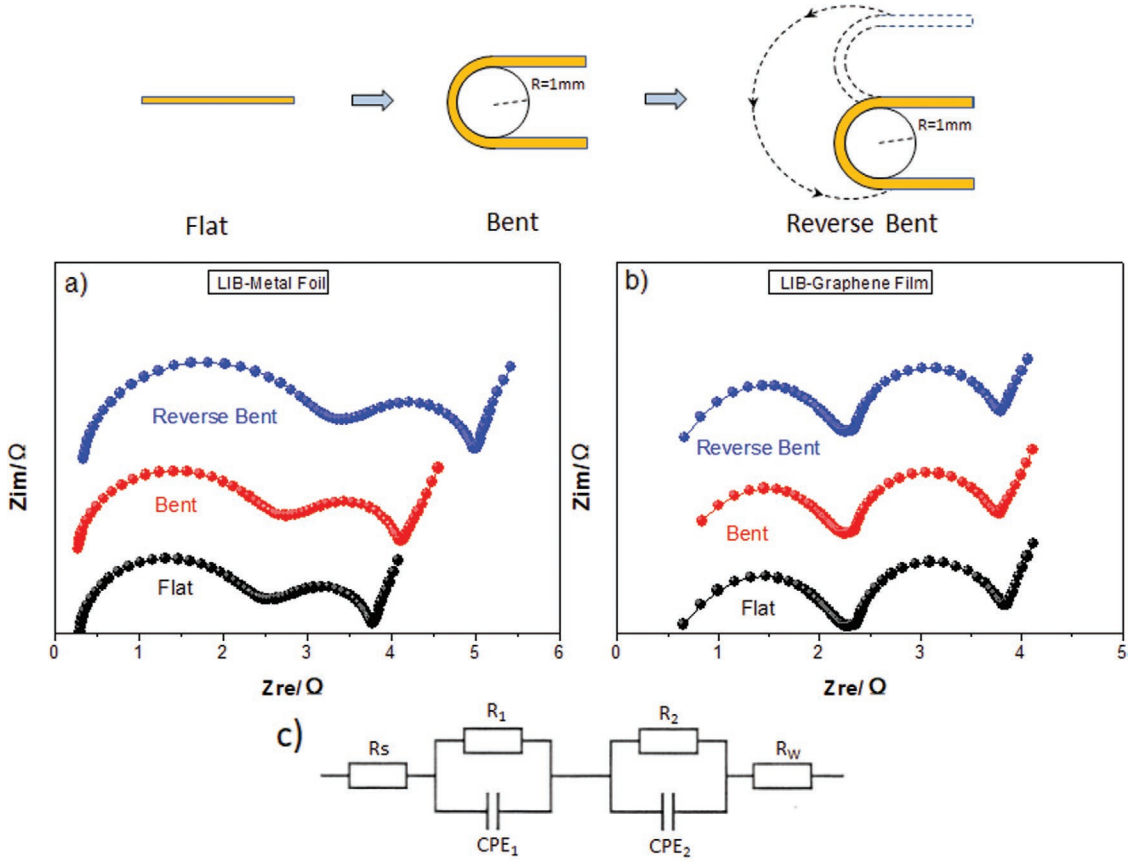

Figure 5. EIS measurements of a) LIB-Metal Foil and b) LIB-Graphene Film at different bending states. c) Equivalent circuit used for simulating the experimental impedance data.

frequency range of 10^6 Hz to 10 mHz at the full charge state (2.8 V). EIS measurements were carried out on the cell at flat, bent, and reverse bent state with a bending radius of 1 mm. All curves included two semicircles, one from high frequency to mid-frequency and the second from mid-frequency to low frequency and a straight line in low frequency. The equivalent circuit is shown in Figure 5c.[62,63] R_s is the electrolyte resistance. The first semicircle denoted as R_1 is due to multiple interfacial resistance within the active layers, which includes the current collector/active layer interface,[64] active material/passivation layer interface,[65] and particle-to-particle interface.[66] Constant phase element (CPE) somehow represents the double-layer capacitance. The second semicircle denoted as R_2 is related to the charge transfer processes between the active particle and the electrolyte. The straight line toward the end of the curve is due to solid state diffusion of lithium ions within the electrode and is represented by R_w.

The comparison of EIS spectroscopies for the cells at flat, bent, and reverse bent state shows that the electrolyte resistance (R_s) and the charge transfer resistance (R_2) are almost constant with continuous bending. However, the first semicircle of LIB-Metal Foil increases after the battery undergoes mechanical bending and reverse bending, which relates to an increase in the interfacial resistance (R_1) within the electrode. As mentioned earlier, R_1 includes the current collector/active layer interfacial resistance. The delamination of active layer from metal foils as shown in Figure 1f could lead to a significant increase in interfacial resistance. Furthermore, it is worthwhile to note that the interfacial resistance (R_1) of LIB-Graphene Film is almost constant under flat, bent, and reverse bent states, further indicating the strong adhesion between the active layer and graphene film. This also exhibits a high consistency with the cross-sectional SEM images of Figure 1g.

The flexibility of LIB-Graphene Film full cell was tested at a speed of 200 mm s^{-1} with bending radius of 1 cm by a specially designed stepper motor (Video S1, Supporting Information). After every 10 000 times mechanical bending, a charge and discharge cycle was tested at 1 C between 1.5 and 2.8 V. **Figure 6**b shows the discharge-specific capacity of the battery after different bending times. Obviously, no capacity loss was observed after the LIB-Graphene Film was bent up to 100 thousand times. These observations demonstrate an excellent electrochemical stability and mechanical robustness for LIB-Graphene Film. To further investigate flexibility of LIB-Graphene Film, an in situ bending test was carried out at a low speed of 5 mm s^{-1}. Approximately 90 times bending were carried out on one electrochemical cycle and the charge/discharge curves are shown in Figure 6c. Overall, there is almost no shift in the charge/discharge curve, further indicating excellent flexibility of LIB-Graphene Film. In earlier reports of literature, the flexible batteries were bent hundreds of times at most and the electrochemical performances had significantly decreased. The comparison of

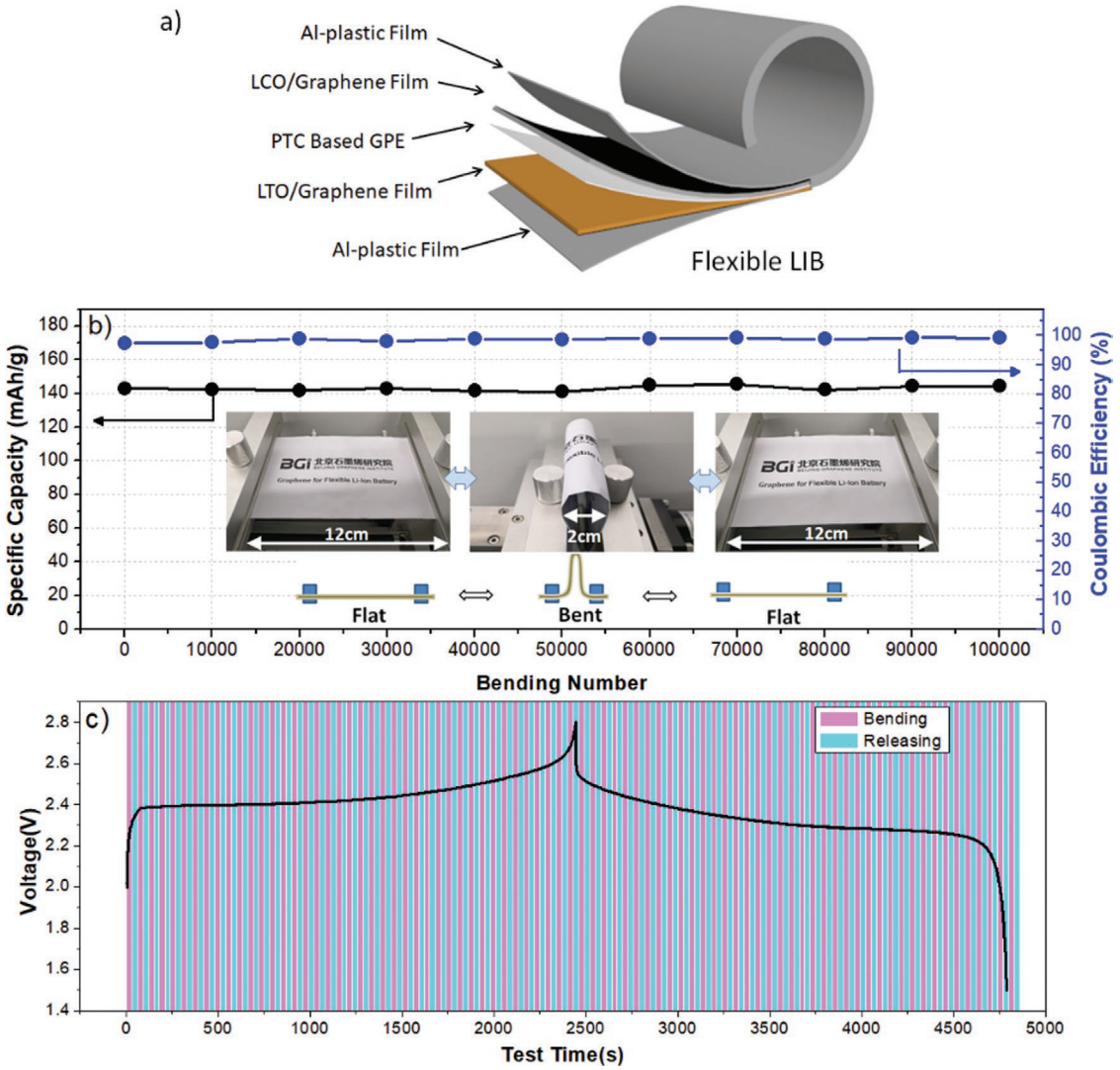

Figure 6. a) Schematic picture of the flexible battery using graphene film as current collector and optimal GO-GPE. b) Cycle performance of the flexible battery cycled at 1C after different bending times. Temperature: 25 °C. Inset: Photographs of the flexible battery before and after bending. c) The charge/discharge curves of flexible battery with in situ ≈90 times mechanical bending.

electrochemical performance with literature reports are exhibited in Table S3, Supporting Information.[15,22,62,67–71] To our knowledge, flexible batteries that could bend so many times have not been reported.

Furthermore, to check the effect of folding on the battery performance, the LIB-Graphene Film flexible battery was tested 100 cycles at 1 C, that is, in the flat state for the first 30 cycles, in the folded state ($R = 1$ mm) for another 40 cycles, and then the flexible battery was unfolded and tested in the flat state in the remaining 30 cycles. The flexible battery exhibited an exciting folding and stability performance, as shown in Figure S8, Supporting Information. A specific capacity of ≈140.4 mAh g^{-1} was obtained after the first cycle, and the capacity retention was ≈98.1% after 100 cycles (Figure S8a, Supporting Information). The specific capacity of the flexible battery was quite insensitive to the folding and unfolding of the battery. Moreover, the charge/discharge curves in the flat state well matched the results in the folded state, including specific capacity and voltage platform (Figure S8b, Supporting Information). These results indicate that the battery performance is mostly unaffected by the folding process.

Figure 7a–c shows optical images of flexible battery connected in series with a green light-emitting diode (LED) (Video S2, Supporting Information). The battery can light the LED continuously under flat state, and still work well under external bended condition with a bending radius of 1 mm. When recovered to the flat state, it was found that the brightness of the LED was constant during this period and could still last for several hours. Moreover, the change in the open circuit voltage of the full cell at charge state was tested under in situ bending conditions (Figure 7d). When using graphene film as current collector, the voltage of LIB-Graphene Film barely dropped under in situ 800 times bending; however, the voltage of LIB-Metal Foil dropped significantly. Therefore, the full cell of LIB-Graphene Film could supply power continuously and steadily without brightness change under bended condition. It is well

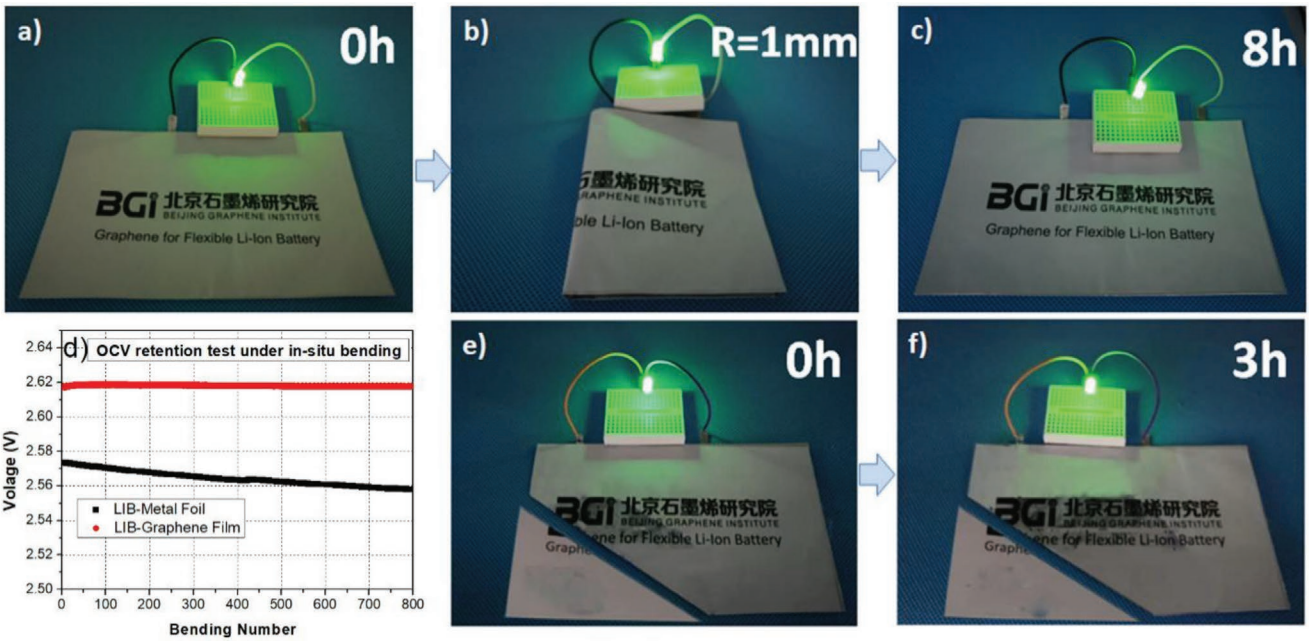

Figure 7. Demonstration of the flexible battery connected in series with a green light-emitting diode (LED) a) when flat, b) after one bending, and c) flattened again and lasting for more than 8 h. d) Plot of open-circuit voltage at full charge state according to bending number in the in situ bending test. e) A corner of the flexible battery is cut off to power an LED and f) lasting for more than 3 h.

known that the delamination of active layer from current collector could lead to the voltage drop.[62] The comparison of voltage drop proved again the excellent flexibility of graphene film and the strong adhesion between the active layer and the graphene film.

To further test the safety of flexible battery, a corner of the flexible battery was cut off to power an LED, as shown in Figure 7e,f. It was observed that the battery can still light an LED and last for more than 3 h without internal short-circuit (Video S3, Supporting Information). Here, it is worthwhile to note that both the reliability and the safety of batteries incorporating GO-GPE were remarkably improved.

3. Conclusions

In conclusion, the present study demonstrates an extremely safe and flexible gel polymer LIB for future scalable applications. Ultra-thin, ultra-light, and highly flexible graphene films are used as current collectors for the LTO anode and LCO cathode. The flexible LIB made of graphene films exhibited exceptional stable performance over 100 thousand times mechanical bending with no capacity loss. The highly flexible graphene films can be bent tens of thousands of times without plastic deformation. More importantly, the strong adhesion between the active layer and the graphene film effectively restrains delamination of active layer under severe bending conditions. The freestanding graphene films minimize the thickness of inactive components within the battery and also enhance both the mass energy density and the power density ≈1.4 times higher than those from standard battery using metal foil current collectors. In addition, the GO-GPE exhibited strong absorption of liquid electrolyte, wide electrochemical window, and superior thermal and electrochemical stability. It also has higher ionic conductivity and higher lithium ion transference number than the commercial Celgard separator. The flexible LIBs using GO-GPE in this paper present excellent safety characteristic even in extremely harsh conditions. It is anticipated that scalable flexible battery with high energy and power density, superior safety, and excellent reliability will provide energy for future wearable electronics and many other applications in extreme and/or conformal conditions.

4. Experimental Section

Sample Collection: Graphene film was purchased from XG Sciences Inc. (XG LeafB). PTC (M_w ≈ 400 000–600 000) was purchased from Wuhan Methyl Technology Co., Ltd. PEO (M_w ≈ 100 000) was supplied by Shanghai Macklin Biochemical Co., Ltd. The GO (sheet diameter of 30–50 µm, thickness of 1.0–1.77 nm, layer numbers of 1–5) powder was purchased from Suzhou Tanfeng Graphene Technology Co., Ltd.

Fabrication of Gel Polymer Electrolyte: GO-GPE was prepared by the means of phase inversion method. First, 0.106 g of GO powder was dispersed in 35 mL DMF for 30 min under ultrasonic dispersion to form a suspension solution. Then 10 g of PTC was dissolved in the obtained suspension solution at 35 °C for 12 h under magnetic stirring to obtain a homogeneous solution. Subsequently, 1 g of PEO was dissolved in 40 mL acetonitrile and stirred at 40 °C for 12 h. Next, the PEO acetonitrile solution was then added into the PTC/GO/DMF solution to get a homogeneous slurry at 35 °C for 12 h under magnetic stirring. The slurry was coated on the surface of clean glass plate by a doctor-blading method, and then transferred into the anhydrous ethanol bath to produce phase inversion. In this process, rapid interdiffusion occurred between ethanol and DMF, and the ethanol molecules gradually occupied the position of DMF solvent molecules to form a wet GO-GPE membrane. The membrane needed to be continuously soaked in the anhydrous ethanol for 3 h to ensure thorough removal of the residual DMF solvent. Finally, the GO-GPE porous membrane was dried

in a vacuum oven for 24 h at 80 °C to remove the solvent and ethanol. In this preparation process, for comparison, pristine P-GPE without GO was also prepared. The as-obtained porous membrane (thickness of 90–110 µm) was immersed into the liquid electrolyte (1.0 M $LiPF_6$ in EC/DEC = 1:1, v/v with 5.0% FEC) for 2 h, ultimately obtaining P-GPE and GO-GPE.

Electrochemical Test for Coin Cell: $LiCoO_2$ (Shenzhen Kejing Star Technology Ltd.) was used as cathode. $Li_4Ti_5O_{12}$ (Shenzhen Kejingstar Technology Ltd.) was used as anode. The electrode was composed of LCO (LTO), super P as the conductive additive, and PVDF as the binder (80:10:10 weight ratio). The LCO slurry was spread onto an Al foil and a graphene film. The LTO slurry was spread onto a Cu foil and a graphene film. The electrodes were dried at 100 °C in vacuum for at least 10 h. Coin cells (2032) were assembled in an Ar-filled glove box using Li foil as the counter electrode. The cathode and anode material loads in each coin cell were typically 4–5 and 5–5.5 mg cm^{-2}, respectively. The electrolyte was 1.0 M $LiPF_6$ in EC/DEC = 1:1, v/v with 5.0% FEC, and commercial polypropylene microporous film (Celgard 2300), P-GPE, and GO-GPE as the separator. The assembled coin cells were cycled at different charge/discharge rates on a Land battery tester (Wuhan Land Electronic Co. Ltd.).

Electrochemical Test for Flexible Battery: Flexible lithium ion battery (full cell) was assembled with LCO as cathode, LTO as anode, graphene film as current collector, and Al-plastic film as packaging materials. For comparison, the full cell using Al foil as positive current collector and Cu foil as negative current collector was also assembled. The anode and cathode electrode areas were 5 cm × 6 cm. Each electrode had the same composition as the corresponding coin cell electrode. GO-GPE was chosen as the separator. The capacity of each full cell was ≈40 mAh and the N/P ratio (negative electrode capacity/positive electrode capacity) was 0.8. The assembled full cells were cycled at different charge/discharge rates at 25 °C on a Land battery tester (Wuhan Land Electronic Co. Ltd.). The galvanostatic charge/discharge was carried out in a voltage window of 1.5–2.8 V.

Electrochemical Evaluation: The ionic conductivity (σ) of commercial Celgard separator and GPEs was characterized by alternating current (AC) impedance method (Autolab, Metrohm) with a potential amplitude of 5 mV using the first applied frequency of 10^6 Hz and the last applied frequency of 0.1 Hz by assembling a coin cell with a symmetrical structure SS|GPE|SS. The ionic conductivity (σ, S cm^{-1}) of commercial Celgard separator and GPE was calculated according to the following equation:[50]

$$\sigma = \frac{d}{SR_b} \tag{1}$$

The vertical distance from one electrode to the other is d (cm); S is the effective area of the commercial Celgard separator and GPEs (cm^2); and the bulk resistance of the Celgard separator and GPEs is R_b (Ω). Coin cells were used to test the lithium-ion migration number (t_+) of Celgard separator and GPEs at room temperature with Li|GPE|Li (Li, lithium metal foil) structures according to Equation (2).[51]

$$t_+ = \frac{I_s(\Delta V - I_0R_0)}{I_0(\Delta V - I_sR_s)} \tag{2}$$

where ΔV is the selected polarization voltage (mV); I_0 is the initial currents (mA), I_s is the steady-state currents; R_0 is the initial resistances (Ω), R_s is the steady-state resistances. The coin cell of Li|PSPE|Li was used to test cell polarization by charge and discharge tests with the constant current of 10 mV s^{-1}.

Characterization Methods: The morphology and microstructure of the samples were examined using SEM (FE-SEM, Zeiss Supra 55). The EIS measurements, open circuit voltage, and cyclic voltammetry analysis were carried out using the Autolab (Metrohm). The specific surface area of the porous membrane was determined from N_2 adsorption isotherms (BELSORP-max, MicrotracBEL). The thickness of graphene film was tested by digimatic indicator (Mitutoyo) with accuracy of 0.001 mm. The bending test was performed by a specially designed stepper motor.

Supporting Information

Supporting Information is available from the Wiley Online Library or from the author.

Acknowledgements

W.S. and K.L. contributed equally to this work. This work was supported by the Beijing Municipal Science & Technology Commission (No. Z181100004818004, No. Z181100001018029, and No. Z191100006119027). The authors also appreciate the technical assistance from the BGI Characterization & Quality Assurance Center.

Conflict of Interest

The authors declare no conflict of interest.

Keywords

flexible batteries, gel polymer electrolytes, graphene, lithium ion batteries

Received: December 31, 2019
Revised: February 28, 2020
Published online: April 20, 2020

[1] M. Armand, J.-M. Tarascon, *Nature* **2008**, *451*, 652.
[2] L. Yang, S. Cheng, Y. Ding, X. B. Zhu, Z. L. Wang, M. L. Liu, *Nano Lett.* **2012**, *12*, 321.
[3] J. A. Rogers, T. Someya, Y. Huang, *Science* **2010**, *327*, 1603.
[4] M. H. Park, K. Kim, J. Kim, J. Cho, *Adv. Mater.* **2010**, *22*, 415.
[5] Y. Liu, Z. Sun, K. Tan, D. K. Denis, J. Sun, L. Liang, L. Hou, C. Yuan, *J. Mater. Chem. A* **2019**, *7*, 4353.
[6] Y. Q. Li, J. C. Li, X. Y. Lang, Z. Wen, W. T. Zheng, Q. Jiang, *Adv. Funct. Mater.* **2017**, *27*, 1700447.
[7] L. N. Cong, H. M. Xie, J. H. Li, *Adv. Energy Mater.* **2017**, *7*, 1601906.
[8] L. Liang, X. Sun, J. Zhang, L. Hou, J. Sun, Y. Liu, S. Wang, C. Yuan, *Adv. Energy Mater.* **2019**, *9*, 1802847.
[9] L. B. Hu, J. W. Chol, Y. Yang, S. Jeong, F. L. Mantia, L. F. Cui, Y. Cui, *Proc. Natl. Acad. Sci. U. S. A.* **2009**, *106*, 21490.
[10] J. Z. Wang, S. L. Chou, H. Liu, G. X. Wang, C. Zhong, S. Y. Chew, H. K. Liu, *Mater. Lett.* **2009**, *63*, 2352.
[11] A. M. Gaikwad, D. A. Steingart, T. N. Ng, D. E. Schwartz, G. L. Whiting, *Appl. Phys. Lett.* **2013**, *102*, 233302.
[12] J. Ren, Y. Zhang, W. Bai, X. Chen, Z. Zhang, X. Fang, W. Weng, Y. Wang, H. Peng, *Angew. Chem.* **2014**, *126*, 7998.
[13] N. Li, Z. Chen, W. Ren, F. Li, H.-M. Cheng, *Proc. Natl. Acad. Sci. U. S. A.* **2012**, *109*, 17360.
[14] Y. Zhang, W. Bai, X. Cheng, J. Ren, W. Weng, P. Chen, X. Fang, Z. Zhang, H. Peng, *Angew. Chem.* **2014**, *126*, 14792.
[15] L. Hu, H. Wu, F. L. Mantia, Y. Yang, Y. Cui, *ACS Nano* **2010**, *4*, 5843.
[16] J. Ren, Y. Zhang, W. Bai, X. Chen, Z. Zhang, X. Fang, W. Weng, Y. Wang, H. Peng, *Angew. Chem., Int. Ed.* **2014**, *53*, 7864.
[17] H. Lee, J. K. Yoo, J. H. Park, J. H. Kim, K. Kang, Y. S. Jung, *Adv. Energy Mater.* **2012**, *2*, 976.

[18] Y. Zhang, W. Bai, X. Cheng, J. Ren, W. Weng, P. Chen, X. Fang, Z. Zhang, H. Peng, *Angew. Chem., Int. Ed.* **2014**, *53*, 14564.
[19] A. H. Whitehead, M. Schreiber, *J. Electrochem. Soc.* **2005**, *152*, A2105.
[20] F. Bonaccorso, L. Colombo, G. Yu, M. Stoller, V. Tozzini, A. C. Ferrari, R. S. Ruoff, V. Pellegrini, *Science* **2015**, *347*, 1246501.
[21] G. M. Zhou, F. Li, H.-M. Cheng, *Energy Environ. Sci.* **2014**, *7*, 1307.
[22] Q. Cheng, Z. Song, T. Ma, B. Smith, R. Tang, H. Yu, H. Jiang, C. K. Chan, *Nano Lett.* **2013**, *13*, 4969.
[23] Z. Song, T. Ma, R. Tang, Q. Cheng, X. Wang, D. Krishnaraju, R. Panat, C. K. Chan, H. Yu, H. Jiang, *Nat. Commun.* **2014**, *5*, 3140.
[24] K. Wang, S. Luo, Y. Wu, X. He, F. Zhao, J. Wang, K. Jiang, S. Fan, *Adv. Funct. Mater.* **2013**, *23*, 846.
[25] D. Wei, P. Hiralal, H. Wang, H. E. Unalan, M. Rouvala, I. Alexandrou, P. Andrew, T. Ryhänen, G. A. J. Amaratunga, *Nano Energy* **2013**, *2*, 1054.
[26] V. L. Pushparaj, M. M. Shaijumon, A. Kumar, S. Murugesan, L. Ci, R. Vajtai, R. J. Linhardt, O. Nalamasu, P. M. Ajayan, *Proc. Natl. Acad. Sci. U. S. A.* **2007**, *104*, 13574.
[27] B. Liu, J. Zhang, X. Wang, G. Chen, D. Chen, C. Zhou, G. Shen, *Nano Lett.* **2012**, *12*, 3005.
[28] L. F. Shen, B. Ding, P. Nie, G. Z. Cao, X. G. Zhang, *Adv. Energy Mater.* **2013**, *3*, 1484.
[29] H. Gwon, H.-S. Kim, K. U. Lee, D.-H. Seo, Y. C. Park, Y.-S. Lee, B. T. Ahn, K. Kang, *Energy Environ. Sci.* **2011**, *4*, 1277.
[30] X. Huang, R. Wang, D. Xu, Z. Wang, H. Wang, J. Xu, Z. Wu, Q. Liu, Y. Zhang, X. Zhang, *Adv. Funct. Mater.* **2013**, *23*, 4345.
[31] N. Li, Z. Chen, W. Ren, F. Li, H.-M. Cheng, *Proc. Natl. Acad. Sci. U. S. A.* **2012**, *109*, 17360.
[32] Y. H. Li, Y. M. Zhao, M. Roe, D. Furniss, Y. Q. Zhu, S. R. P. Silva, J. Q. Wei, D. H. Wu, C. H. P. Poa, *Small* **2006**, *2*, 1026.
[33] W. J. Ma, L. Song, R. Yang, T. H. Zhang, Y. C. Zhao, L. F. Sun, Y. Ren, D. F. Liu, L. F. Liu, J. Shen, Z. X. Zhang, Y. J. Xiang, W. Y. Zhou, S. S. Xie, *Nano Lett.* **2007**, *7*, 2307.
[34] J. Ma, Samsung has released the results of its investigation into the exploding galaxy Note7, http://www.xinhuanet.com//fortune/2017-01/24/c_1120371367.htm (accessed: January 2017).
[35] Fox, A Tesla Model S has reignited in Hong Kong, http://www.techweb.com.cn/world/2019-05-14/2735691.shtml (accessed: May 2019).
[36] P. Hovington, M. Lagace, A. Guerfi, P. Bouchard, A. Mauger, C. M. Julien, M. Armand, K. Zaghib, *Nano Lett.* **2015**, *15*, 2671.
[37] S. A. Theron, E. Zussman, A. L. Yarin, *Polymer* **2004**, *45*, 2017.
[38] P. Raghavan, J. Manuel, X. Zhao, D. S. Kim, J. H. Ahn, C. Nah, *J. Power Sources* **2011**, *196*, 6742.
[39] J. A. Galloway, K. J. Koester, B. J. Paasch, C. W. Macosko, *Polymer* **2004**, *45*, 423.
[40] A. Martinelli, M. A. Navarra, A. Matic, S. Panero, P. Jacobsson, L. Börjesson, B. Scrosati, *Electrochim. Acta* **2005**, *50*, 3992.
[41] S. Ramesh, A. K. Arof, J. Structural, *J. Power Sources* **2001**, *99*, 41.
[42] S. Ahmad, S. Ahmad, S. A. Agnihotry, *J. Power Sources* **2005**, *140*, 151.
[43] H. S. Kim, P. Periasamy, S. I. Moon, *J. Power Sources* **2005**, *141*, 293.
[44] Z. H. Li, P. Zhang, H. P. Zhang, Y. P. Wu, X. D. Zhou, *Electrochem. Commun.* **2008**, *10*, 791.
[45] J. Xi, X. Qiu, J. Li, X. Tang, W. Zhu, L. Chen, *J. Power Sources* **2006**, *157*, 501.
[46] S. Zhang, N. Zhang, C. Huang, K. Ren, Q. M. Zhang, *Adv. Mater.* **2005**, *17*, 1897.
[47] Y. C. Li, J. Schulz, S. Mannen, C. Delhom, B. Condon, S. Chang, M. Zammarano, J. C. Grunlan, *ACS Nano* **2010**, *4*, 3325.
[48] T. Liu, M. Zhang, Y. L. Wang, Q. Y. Wang, C. Lv, K. X. Liu, S. Suresh, Y. H. Yin, Y. Y. Hu, Y. S. Li, X. B. Liu, S. W. Zhong, B. Y. Xia, Z. P. Wu, *Adv. Energy Mater.* **2018**, *8*, 1802349.
[49] W. Wang, Q. Xu, H. Liu, Y. Wang, Y. Xia, *J. Mater. Chem. A* **2017**, *5*, 8440.
[50] Y. Choi, K. Zhang, K. Y. Chung, D. H. Wang, J. H. Park, *RSC Adv.* **2016**, *6*, 80706.
[51] T. Kashiwagi, F. Du, J. F. Douglas, K. I. Winey, R. H. Harris Jr., J. R. Shields, *Nat. Mater.* **2005**, *4*, 928.
[52] H. D. Wagner, *Nat. Nanotechnol.* **2007**, *2*, 742.
[53] G. Chen, F. Zhang, Z. Zhou, J. Li, Y. Tang, *Adv. Energy Mater.* **2018**, *8*, 1801219.
[54] X. Yang, F. Zhang, L. Zhang, T. F. Zhang, Y. Huang, Y. S. Chen, *Adv. Funct. Mater.* **2013**, *23*, 3353.
[55] S. Y. Yang, R. Benitez, A. Fuentes, K. Lozano, *Compos. Sci. Technol.* **2007**, *67*, 1159.
[56] C. Y. Chiang, Y. J. Shen, M. J. Reddy, P. P. Chu, *J. Power Sources* **2003**, *123*, 222.
[57] Y. Saito, H. Kataoka, E. Quartarone, P. Mustarelli, *J. Phys. Chem. B* **2002**, *106*, 7200.
[58] Z. Y. Cui, Y. Y. Xu, L. P. Zhu, J. Y. Wang, Z. Y. Xi, B. K. Zhu, *J. Membr. Sci.* **2008**, *325*, 957.
[59] C. E. Lin, H. Zhang, Y. Z. Song, Y. Zhang, J. J. Yuan, B. K. Zhu, *J. Mater. Chem. A* **2018**, *6*, 991.
[60] Y.-M. Chen, S.-T. Hsu, Y.-H. Tseng, T.-F. Yeh, S.-S. Hou, J.-S. Jan, Y.-L. Lee, H. Teng, *Small* **2018**, *14*, 1703571.
[61] C.-H. Tsao, P.-L. Kuo, *J. Membr. Sci.* **2015**, *489*, 36.
[62] A. M. Gaikwad, B. V. Khau, G. Davies, B. Hertzberg, D. A. Steingart, A. C. Arias, *Adv. Energy Mater.* **2015**, *5*, 1401389.
[63] S. S. Zhang, K. Xu, T. R. Jow, *Electrochim. Acta* **2006**, *51*, 1636.
[64] M. Gaberscek, J. Moskon, B. Erjavec, R. Dominko, J. Jamnik, *Electrochem. Solid-State Lett.* **2008**, *11*, A170.
[65] S. S. Zhang, K. Xu, T. R. Jow, *Electrochim. Acta* **2004**, *49*, 1057.
[66] H. Zheng, L. Tan, G. Liu, X. Song, V. S. Battaglia, *J. Power Sources* **2012**, *208*, 52.
[67] Z. Wang, Z. Wu, N. Bramnik, S. Mitra, *Adv. Mater.* **2014**, *26*, 970.
[68] J. W. Hu, Z. P. Wu, S. W. Zhong, W. B. Zhang, S. Suresh, A. Mehta, N. Koratkar, *Carbon* **2015**, *87*, 292.
[69] S. Xu, Y. Zhang, J. Cho, J. Lee, X. Huang, L. Jia, J. A. Fan, Y. Su, J. Su, H. Zhang, H. Cheng, B. Lu, C. Yu, C. Chuang, T. I. Kim, T. Song, K. Shigeta, S. Kang, C. Dagdeviren, I. Petrov, P. V. Braun, Y. Huang, U. Paik, J. A. Rogers, *Nat. Commun.* **2013**, *4*, 1543.
[70] M. H. Park, M. Noh, S. Lee, M. Ko, S. Chae, S. Sim, S. Choi, H. Kim, H. Nam, S. Park, J. Cho, *Nano Lett.* **2014**, *14*, 4083.
[71] X. Fang, C. F. Shen, M. Y. Ge, J. P. Rong, Y. H. Liu, A. Y. Zhang, F. Wei, C. W. Zhou, *Nano Energy* **2015**, *12*, 43.